

NOMTO: Neural Operator-based symbolic Model approximaTion and discOvery

Sergei Garmaev¹, Siddhartha Mishra², and Olga Fink¹

¹IMOS Laboratory, EPFL, Lausanne, Switzerland

²Seminar for Applied Mathematics, ETH AI Center, ETH, Zurich, Switzerland

December 2024

Abstract

While many physical and engineering processes are most effectively described by non-linear symbolic models, existing non-linear symbolic regression (SR) methods are restricted to a limited set of continuous algebraic functions, thereby limiting their applicability to discover higher order non-linear differential relations. In this work, we introduce the Neural Operator-based symbolic Model approximaTion and discOvery (NOMTO) method, a novel approach to symbolic model discovery that leverages Neural Operators to encompass a broad range of symbolic operations. We demonstrate that NOMTO can successfully identify symbolic expressions containing elementary functions with singularities, special functions, and derivatives. Additionally, our experiments demonstrate that NOMTO can accurately rediscover second-order non-linear partial differential equations. By broadening the set of symbolic operations available for discovery, NOMTO significantly advances the capabilities of existing SR methods. It provides a powerful and flexible tool for model discovery, capable of capturing complex relations in a variety of physical systems.

1 Main

Many physical and engineering processes are most effectively described by concise mathematical expressions derived through meticulous observation and analysis. The accuracy of these models is highly dependent on the quality and quantity of available data. With the emergence of large-scale datasets across diverse physical and engineering domains, deriving compact mathematical models in the form of symbolic expressions has become increasingly attainable. This methodology, known as symbolic regression (SR), aims to identify mathematical expressions that most accurately represent given datasets. SR has become indispensable in fields such as physics, biology, and engineering, where it advances knowledge and fosters innovation by uncovering underlying principles and facilitating the development of interpretable predictive models.

In recent years, deep learning-based approaches have significantly advanced the field of SR by leveraging neural networks to identify mathematical expressions directly from data. Techniques based on transformer architectures and reinforcement learning [1, 2, 3] have expanded SR's capabilities by incorporating advanced deep learning strategies. For example, reinforcement learning facilitates more adaptive and flexible model discovery processes [1, 4], while transformer-based approaches have demonstrated effectiveness in capturing complex dependencies within data [5]. These model-based approaches require extensive training on the data labeled with known governing symbolic expressions prior to inferring another symbolic expressions. Despite these advancements, such methods often struggle to generalize to out-of-distribution equations and require extensive training datasets [6].

In contrast to model-based approaches, search-based SR methods [7] do not require extensive training datasets and can effectively operate in out-of-distribution domains [6]. These methods directly manipulate symbolic operations directly and are not restricted to the set of functions used during training, distinguishing them from model-based approaches. Among search-based techniques, genetic programming, stands out as a prominent method. It evolves populations of candidate solutions through genetic operators such as crossover and mutation [8, 6], representing mathematical expressions as sequences of variables, constants, and operators. Genetic programming has been widely applied as a model discovery tool across a wide range of disciplines, including astronomy [9, 10], materials science [11, 12], and medical sciences [13, 14]. However, genetic programming is inherently heuristic and often lacks systematic exploration of the solution space. Unlike gradient-based optimization techniques, which offer a more direct and efficient path to optimal solutions, genetic programming relies on evolutionary strategies that are less targeted and more exploratory [6, 15]. These limitations become particularly pronounced in high-dimensional datasets and when dealing with complex mathematical operations, ultimately constraining the effectiveness and scalability of genetic programming-based methods [1].

To address these challenges, alternative approaches that incorporate domain knowledge into the exploration of the solution space have become increasingly desirable. One promising method, the Sparse Identification of Nonlinear Dynamical Systems (SINDy) algorithm [16], enhances the search process by solving the task as a linear regression on the set of manually defined combinations of input variables. While SINDy is valued for its simplicity and ease of implementation [17], it fundamentally relies on linear regression and requires manual selection of library functions and their combinations, limiting its applicability, particularly in scenarios where domain insights are scarce or unavailable. Therefore, algorithms capable of automatically searching for nonlinear combinations of input variables without manual selection are preferable and can be categorized as nonlinear symbolic regression methods.

One example of nonlinear symbolic regression methods are the Equation Learner (EQL) algorithm [18], which utilizes a conventional neural network architecture by substituting traditional activation functions with a predefined set of library functions to derive symbolic expressions through sparse weight optimization. Similarly, the recently proposed Kolmogorov-Arnold Networks (KANs) substitute conventional non-linear activations with learnable activation functions [19], making them a suitable scientific discovery tool for time series [20] and algebraic terms of ordinary differential equations (ODEs) [21]. The key difference between KANs and EQL lies in their symbolic operation construction process, where KANs match the learnable activation functions to the most similar library function at the post-processing stage. In contrast, the EQL algorithm initially constructs a network composed of exact library functions. Despite their flexible architectures, both EQL and KANs encounter significant limitations. They particularly struggle with operations involving singularities, such as division or exponential functions, which are essential for accurately modeling real-world phenomena. Additionally, these algorithms have limited capacity to incorporate more complex operations, making them unsuitable for model discovery tasks that involve special functions or differential operators.

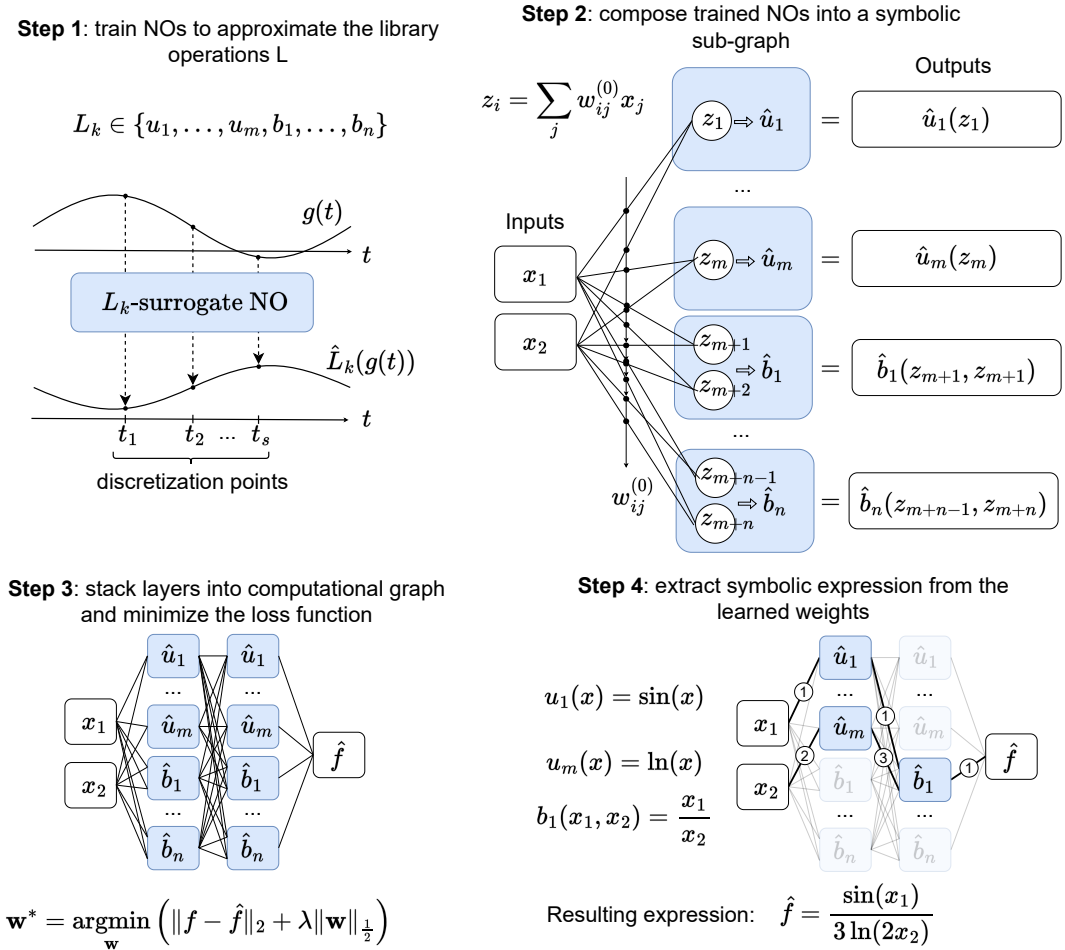


Figure 1: The general implementation steps and architecture of the Neural Operator-based symbolic Model approximation and discOverY (NOMTO) algorithm.

To overcome these limitations, we propose a novel symbolic regression method that leverages neural operators to automatically identify various non-linear combinations of input variables, incorporating special functions and differential operators [22, 23, 24]. We designate this approach as Neural Operator-based symbolic Model

approximation and discovery (NOMTO¹). Compared to heuristic-based techniques, NOMTO leverages gradients provided by surrogate neural operators to explore the solution space, making the search more efficient. Moreover, the proposed algorithm, as we will demonstrate, is able to discover non-linear partial differential equations. NOMTO operates as a computational graph encompassing all potential non-linear combinations of symbolic operations up to a specified depth (Figure 1, Step 3). Neural operators, pre-trained to approximate symbolic operations, serve as nodes within the computational graph. Each edge in graph is assigned a scalar weight, acting as multiplier coefficient for the corresponding node’s output. By minimizing the discrepancy between the outputs of the computational graph and the target expression’s values, NOMTO approximates the desired dependency as a non-linear combination of the input variables. Additionally, an extra penalty term enforces sparsity in the edge weights, enabling NOMTO to construct compact and interpretable symbolic expressions.

The core components of NOMTO are surrogate neural operators, specifically the Fourier Neural Operator (FNO) [25] and the Convolutional Neural Operator (CNO) [23], employed in this study. Neural operators typically operate within functional spaces, meaning their inputs and outputs of neural operator consist of discretized functions. We distinguish between these input/output functions of the neural operators and the symbolic operations that form the final symbolic expression. The set of symbolic operations can contain various algebraic functions, differential operators, and special functions, which we refer to as the library. The neural operators are first pre-trained to approximate each operation in the library (Fig. 1, Step 1). The training data consists of random input functions discretized at a set of fixed points, with corresponding outputs generated by applying the exact library operations point-wise to these discretized input functions. After training, the neural operators are integrated into a computational sub-graph that represents a linear combination of library operations applied to the weighted sums of the input variables (Fig. 1, Step 2). These computational sub-graphs are subsequently stacked to form a comprehensive computational graph capable of representing all non-linear combinations of the input variables involving the library functions, up to the desired expression tree depth (Fig. 1, Step 3). Each node in the resulting symbolic expression is computed by applying the corresponding library operation to the weighted sum of outputs from preceding nodes. Thus, the final symbolic expression at the output node is derived by recursively extracting expressions from the preceding nodes. Optimization involves learning the graph weights while the neural operator surrogates remain frozen. To ensure the resulting expression remains compact, we enforce sparsity on the weights using the $\ell_{1/2}$ -norm applied jointly to all weights. Additionally, we optionally employ a periodic pruning technique in experiments, where the set of NOMTO weights is substantially large. The optimization process is detailed in Section 4.3. Once optimization is complete, the final symbolic expression is extracted from the optimized set of weights. Figure 1 (Step 4) illustrates an example of a possible NOMTO outcome.

By extending the range of symbolic operations beyond algebraic functions, NOMTO represents a significant advancement in the field of symbolic regression. Its key contributions include:

- A novel approach to construct and dynamically refine non-linear symbolic expressions by leveraging gradients provided by neural operators.
- Robust handling of singularities through surrogate neural operators trained on redefined versions of problematic functions.
- Discovering non-linear partial differential equations directly from observation data without the need for manually constructing non-linear combinations.

NOMTO’s ability to discover governing models directly from observations makes it as a promising tool for model discovery across various disciplines, including fluid dynamics, materials science, biological systems modeling, and climate science.

2 Results

We evaluated the performance of the proposed NOMTO algorithm on symbolic regression tasks using a representative selection of symbolic expressions from the Nguyen [26] and Keijzer [27] benchmark sets. Beyond elementary expressions, we extended our evaluation to expressions containing differential operators and special functions, demonstrating NOMTO’s unique ability to handle tasks where other SR algorithms typically fail. Furthermore, we showcase the algorithm’s performance in model discovery tasks, successfully recovering the governing equations of two systems: a two-dimensional diffusion system governed by the heat equation and a two-dimensional advection-diffusion system governed by the Burgers’ equations.

¹The name Nomto is derived from the Buryat-Mongolian language, translating to “educated” or “wise”, which reflects the algorithm’s intelligent exploration of the symbolic solution space.

2.1 Symbolic Regression Task

To assess NOMTO’s effectiveness in symbolic regression, we compared its performance with state-of-the-art methods, EQL and KAN. This comparison aims to evaluate the impact of employing neural operators in NOMTO’s computational graph, contrasting them with the exact operations used in EQL and the learnable activation functions in KAN.

The symbolic expressions chosen for this evaluation ensure a representative mix of various symbolic operations (Table 1). For a fair comparison, we prepared consistent datasets that satisfy the input data requirements for different algorithms. EQL and KAN use point-wise input data, while NOMTO operates on discretized functions.

Table 1: Performance comparison (MSE/R^2) on the chosen benchmark expressions (Nguyen and Keijzer).

Expression	EQL	KAN	NOMTO-FNO	NOMTO-CNO
Nguyen-1	$8.7 \cdot 10^{-7} / 1.0$	0.3192 / 0.6808	0.00063 / 0.9992	0.0347 / 0.9561
Nguyen-2	$4.4 \cdot 10^{-6} / 1.0$	0.0016 / 0.9984	0.0007 / 0.9992	0.0474 / 0.9419
Nguyen-5	0.8078 / 0.1923	0.9909 / 0.0091	0.9251 / -0.0108	0.9204 / -0.0270
Nguyen-6	0.2742 / 0.7258	1.1844 / -0.1844	0.5363 / 0.3566	0.8268 / 0.0283
Nguyen-7	0.0123 / 0.9877	0.1407 / 0.8593	0.0396 / 0.9604	0.0328 / 0.9672
Nguyen-8	0.0159 / 0.9842	1.9184 / -0.9184	0.0157 / 0.9843	0.0148 / 0.9852
Keijzer-5	6.5315 / -5.5315	1.0972 / -0.0972	1.0768 / -81.9485	1.7058 / -191.9737
Keijzer-14	0.4391 / 0.5609	1.0242 / -0.0242	0.1465 / 0.8151	0.5962 / 0.4162

For each symbolic expression, we generated 100 random functions by creating mixtures of Gaussians evaluated at the set of 100 equidistant points within the interval $[-10, 10]$. These values served as independent variables, with outputs computed using the benchmark expressions. This process resulted in a training dataset comprising 100 function samples for the NOMTO-based algorithms and 10,000 data points for EQL and KAN. For expressions with undefined regions, the affected data points were excluded from the training dataset for EQL and KAN, while NOMTO excluded undefined discretization points from its loss calculation. Multivariate benchmark expressions, such as Keijzer-5 and Keijzer-14, were supplemented with additional random Gaussians mixtures for the second and third independent variables. To prevent numerical overflow during the optimization, we clipped the output values of all samples to lie within the interval $[-100, 100]$. The number of layers in NOMTO is set to 2. For the Nguyen-5 and Keijzer-5 benchmarks, each model was configured with three layers. In this experiment, all algorithms aimed to discover symbolic expressions by minimizing the discrepancy between their predicted outputs and the reference values.

Table 2: Benchmark expressions recovered by NOMTO-FNO and NOMTO-CNO.

Benchmark	Ground Truth	Recovered Expression
Nguyen-1	$x^3 + x^2 + x$	NOMTO-FNO: $x^3 + x^2 + x$ NOMTO-CNO: $0.7x^3 + 4.0x$
Nguyen-2	$x^4 + x^3 + x^2 + x$	NOMTO-FNO: $0.92x^4 + 3.4x^{2.5} + 3.1x + 2.1$ NOMTO-CNO: $x^4 + 2.0x^2 + 7.6$
Nguyen-5	$\sin(x^2) \cos(x) - 1$	NOMTO-FNO: $-0.4 \sin(0.4 \cos^2(x - 1.0)) - 1.0$ NOMTO-CNO: $0.1 \cos(2.0 \ln(x) + 0.9) - 0.9$
Nguyen-6	$\sin(x) + \sin(x + x^2)$	NOMTO-FNO: $\sin(x + 0.9 \sin(x) - 0.2 \cos(x)) + 0.3$ NOMTO-CNO: $\sin(0.5 \ln(-x) - 2.2) - 0.5 \cos^2(x) + 0.8$
Nguyen-7	$\ln(x + 1) + \ln(x^2 + 1)$	NOMTO-FNO: $0.8\sqrt{x} + 0.4x - 0.6 \cos(0.7x) + 0.5 \cos(\cos(0.7x)) + 0.3$ NOMTO-CNO: $2.0\sqrt{x} + 0.4 \sin(\ln(-x) - 0.6) - 0.2$
Nguyen-8	\sqrt{x}	NOMTO-FNO: $0.3\sqrt{x} + 0.1x + 0.8$ NOMTO-CNO: $0.7\sqrt{x} + 0.4$
Keijzer-5	$\frac{30xz}{(x-10)y^2}$	NOMTO-FNO: $\frac{30z^2}{(-x+0.9y+0.07z)^2}$ NOMTO-CNO: $\frac{50xz}{0.1x-0.1y+1.0} + 21.0$
Keijzer-14	$\frac{8}{(2+x^2+y^2)}$	NOMTO-FNO: $\sqrt{-0.5x^2 - 0.1y^2 + \cos(y)} + 0.3$ NOMTO-CNO: $-0.0001x^4 - 0.03x^2 - 0.01y^2 + 0.9$

NOMTO demonstrated performance comparable to EQL and KAN across most benchmark expressions. Table 1 presents the mean squared error (MSE) and coefficient of determination (R^2) achieved on the test expressions. Table 2 showcases the specific expressions recovered by NOMTO-FNO and NOMTO-CNO, while the expressions identified by EQL and KAN are provided in Appendix A. For polynomial functions, the expressions recovered by NOMTO-FNO closely match the ground truth. However, for expressions with lower mean magnitudes, such as Nguyen-5 and Nguyen-6, NOMTO struggles to approximate them precisely, likely due to approximation errors inherited from the underlying neural operators. In the case of Nguyen-7, the algorithm replaced logarithmic dependencies with combinations of square roots, sine and cosine functions while maintaining a low approximation error. Additionally, NOMTO successfully identified the presence of a square root combined with linear dependencies and constants in the Nguyen-8 expression.

For more complex expressions like Keijzer-14, which involve division operations without discontinuities, NOMTO demonstrates strong performance by effectively approximating the true structure. However, for Keijzer-5, which contains discontinuities, all algorithms, including NOMTO, encounter difficulties, highlighting the inherent challenges posed by such functions. Between the two NOMTO variants, NOMTO-FNO outperforms NOMTO-CNO in handling division operations, likely due to superior surrogate accuracy in approximating the jumps in the output functions. Interestingly, NOMTO-CNO also identified a division operation in the resulting expression, likely due to averaging of different training samples.

2.2 Expressions with Derivatives and Special Functions

In this experiment, we evaluate NOMTO’s ability to discover expressions involving derivatives and special functions, such as the Airy function Ai and the gamma function Γ . Discovery of these operations has been challenging for existing non-linear symbolic regression methods. To showcase this capability, NOMTO was applied to identify expressions containing not only algebraic operations but also derivatives and special functions. The test set of expressions, detailed in Table 3, includes one-dimensional derivatives $\frac{d}{dt}$, Ai , and Γ . For this experiment, the independent variable $x_1 = x_1(t)$ was modeled as a randomly generated function of t . The ground truth values of the test expressions were computed point-wise for special functions, while derivatives were numerically calculated with respect to t over the interval $t \in [-10, 10]$.

Table 3: Discovery of symbolic expressions containing 1-dimensional derivatives using NOMTO.

True expression	MSE	R^2	Predicted expression
NOMTO-FNO			
$f_1(x_1) = 4\frac{d}{dt}x_1 + x_1$	0.002	0.995	$4.0\frac{dx_1}{dt} + 1.0x_1 - 0.08\frac{d^2}{dt^2}x_1$
$f_2(x_1, x_2) = 2\sin(x_1)\frac{dx_2}{dt}$	0.957	-0.05	$0.005\frac{dx_1}{dt}\frac{dx_2}{dt} + 0.002\frac{dx_1}{dt} - 0.09\left(\frac{dx_2}{dt}\right)^2 - 0.04\frac{dx_2}{dt}$
$f_3(x_1, x_2) = 3\frac{dx_1}{dt}\frac{dx_2}{dt}$	0.023	0.864	$3.0\frac{dx_1}{dt}\frac{dx_2}{dt}$
$f_4(x_1, x_2) = 6\frac{d}{dt}\left(\frac{x_1}{x_2}\right)$	0.99	0.038	$\frac{1.0\frac{d}{dt}4.0x_1}{x_2} - 1.0Ai(1.0 - 3.0x_2)$
$f_5(x_1, x_2) = 5\frac{d^2x_1}{dt^2}$	0.028	0.957	$5.0\frac{d^2}{dt^2}x_1$
$f_6(x_1) = 5Ai(x_1) + 3x_1$	0.005	0.994	$4.0Ai(-0.7x_1 - 4.0Ai(-0.6x_1)) + 1.0Ai(-0.6x_1) + 3.0x_1 + 0.8\sin(0.2x_1)$
$f_7(x_1) = 2\Gamma(x_1)$	0.209	0.763	$2.0\Gamma(1.0x_1) + 2.0\sin(0.6x_1 + 2.0\sin(0.6x_1) + 2.0Ai(-1.0x_1)) - 0.5\Gamma(-3.0\sin(0.6x_1)) + 0.3$
NOMTO-CNO			
$f_1(x) = 4\frac{d}{dt}x + x$	0.002	0.995	$4.0\frac{dx_1}{dt} + 1.0x_1$
$f_2(x_1, x_2) = 2\sin(x_1)\frac{dx_2}{dt}$	0.958	-0.051	$-0.09\left(\frac{dx_2}{dt}\right)^2 - 0.03\frac{dx_2}{dt} - 0.001$
$f_3(x_1, x_2) = 3\frac{dx_1}{dt}\frac{dx_2}{dt}$	0.02	0.882	$3.0\frac{dx_1}{dt}\frac{dx_2}{dt}$
$f_4(x_1, x_2) = 6\frac{d}{dt}\left(\frac{x_1}{x_2}\right)$	0.986	-0.04	$-\frac{2.0x_1\frac{dx_2}{dt}}{x_2^2} - 0.1 + \frac{2.0\frac{dx_1}{dt}}{x_2}$
$f_5(x_1, x_2) = 5\frac{d^2x_1}{dt^2}$	0.025	0.963	$5.0\frac{d^2}{dt^2}x_1 + 0.03\frac{d}{dt}x_1$
$f_6(x_1) = 5Ai(x_1) + 3x_1$	0.006	0.993	$4.0Ai(-0.6x_1 - 4.0Ai(-0.2x_1)) + 3.0x_1 + 0.9\sin(0.2x_1)$
$f_7(x_1) = 2\Gamma(x_1)$	0.205	0.773	$2.0\Gamma(1.0x_1) + 2.0\sin(0.1x_1 + 0.5) - 0.9\sin(0.7x_1)\Gamma(1.0x_1) + 0.3$

In this experiment, the library comprised the following operations: $\{id, \times, \div, \frac{d}{dt}, \frac{d^2}{dt^2}, \sin, Ai, \Gamma\}$. Neural operator models were trained to approximate these library operations over the interval $[-10, 10]$. The trained neural operators were then integrated into a two-layer NOMTO computational graph. Additionally, we employed the periodic pruning technique detailed in Section 4.3.

Consistent with the previous experiment, the resulting expressions were evaluated using the mean squared error (MSE) and R^2 as presented in Table 3. The NOMTO algorithm effectively approximated these expressions

through straightforward combinations of the library functions, correctly identifying the main components of the ground truth expressions. However, the predicted expressions did not always replicate the structure of the ground truth, even in cases where the approximation error was low.

Interestingly, NOMTO successfully captured the structure of expressions containing the derivative of the division operation and the Γ -function. However, the coefficients of the discovered expressions did not precisely match the ground truth coefficients. This discrepancy results from pre-processing steps that clipped label values between -100 and above 100, thereby preventing precise loss calculation for high magnitude values during the optimization process. Additionally, the neural operators within the NOMTO framework inherited approximation errors that accumulated during optimization, potentially reducing performance on expression f_2 . We attribute this to the low magnitudes of the expression values, which amplify the impact neural operator approximation errors during optimization.

2.3 Governing equations rediscovery

2.3.1 Two-dimensional Heat Equation

In this experiment, we demonstrate NOMTO’s ability to rediscover the partial differential equation governing a two-dimensional diffusion system using simulation data. We compared the performance of two different NOMTO variants, one utilizing FNO and the other CNO as surrogate models.

The training data were generated by numerically solving the heat equation within a two-dimensional rectangular domain. A detailed description of the data preparation process is provided in Appendix B. Each training sample has dimensions (50, 50, 50), corresponding to discretization points along the x -, y - and t -axes. We conducted a total of 1,000 simulations with randomly sampled initial conditions to ensure diversity within the training dataset.

The original two-dimensional heat equation contains two second-order partial derivatives. To assess NOMTO’s capability to handle three-dimensional arrays (i.e., two spatial coordinates and time), we selected a minimal set of library operations – $\{\frac{\partial}{\partial x}, \frac{\partial}{\partial y}\}$. The surrogate neural operators were trained on a grid matching the simulation grid. The FNO surrogates were configured with three layers, four modes, and 32 hidden channels, whereas the CNO models comprised four layers, each containing four residual blocks and a channel multiplier of 32. The training dataset consisted of random three-dimensional mixtures of Gaussians, discretized on the grid of the simulated system to ensure compatibility between the training data and simulation data. The NOMTO algorithm’s computational graph was designed with a depth of two. The input to NOMTO was a three-dimensional tensor representing the temperature field u , and the ground truth output was the three-dimensional tensor $\frac{\partial u}{\partial t}$, with the time derivative calculated numerically using second-order central differences. NOMTO was trained to minimize the loss function:

$$\mathcal{L} = \left\| \frac{\partial u}{\partial t} - \frac{\hat{\partial} u}{\partial t} \right\| + \left\| \sum_{i,j} w_{i,j} \right\|_{1/2}, \quad (1)$$

where $\frac{\hat{\partial} u}{\partial t}$ represents the outputs of NOMTO, and $w_{i,j}$ are the weights on the edges of the computational graph. Since the initial computational graph in this experiment contained at most eight edges, we did not apply any additional pruning during the optimization process. The resulting expressions discovered by the two algorithms are presented in Figure 2.

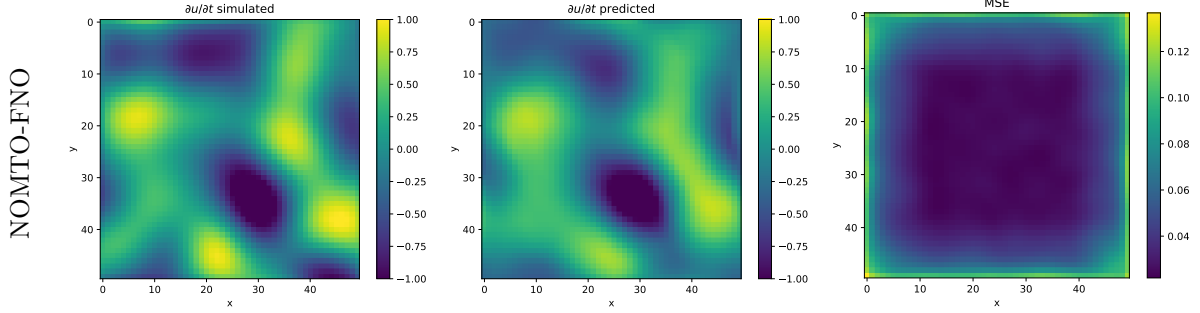
The coefficients of the expressions identified by NOMTO closely matched those of the original heat equation, accurate to the first decimal place. However, NOMTO-FNO variant exhibited slightly higher errors compared to the NOMTO-CNO variant. This discrepancy is likely attributable to the inherent approximation errors in the FNO surrogate models.

Figure 2 demonstrates that NOMTO’s predictions of $\frac{\partial u}{\partial t}$ closely follow the true dynamics, with residuals remaining negligible across most of the simulation domain. This indicates that NOMTO effectively captures the underlying behavior of the heat equation, showcasing its capability to accurately model complex physical systems. However, as depicted in Figure 2, errors are more pronounced near the domain boundaries for NOMTO-FNO compared to the NOMTO-CNO variant. This discrepancy is likely due to inherent approximation errors in FNO surrogates. Enhancing the accuracy of the surrogate models could further reduce prediction errors and improve the precision of the determined coefficients.

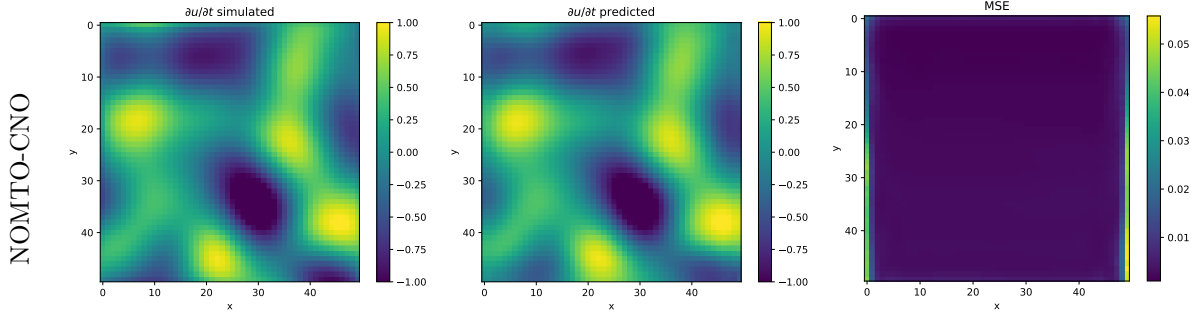
2.3.2 Two-dimensional Burgers’ Equation

In a subsequent experiment, we applied the NOMTO algorithm to rediscover the Burgers’ equation. Unlike the heat equation, Burgers’ equation incorporates both diffusion and convection terms, introducing additional complexity for the NOMTO algorithm. We generated simulation data by solving the two-dimensional Burgers’ equation within a square domain. Detailed simulation parameters and procedures are provided in Appendix C.

Discovered model: $\frac{\partial u}{\partial t} = 1.03 \frac{\partial^2 u}{\partial x^2} + 1.01 \frac{\partial^2 u}{\partial y^2}$. **MSE = 0.058**



Discovered model: $\frac{\partial u}{\partial t} = 1.0 \frac{\partial^2 u}{\partial x^2} + 1.0 \frac{\partial^2 u}{\partial y^2}$. **MSE = 0.004**



(a)

(b)

(c)

Figure 2: Heat equation rediscovery results: The top row presents the outcomes from NOMTO-FNO; while the bottom row shows results from NOMTO-CNO. Panel (a) displays the ground truth $\frac{\partial u}{\partial t}$ obtained through numerical simulation. Panel (b) illustrates the $\frac{\partial u}{\partial t}$ predictions generated by the NOMTO algorithm. Panel (c) depicts the MSE distribution across the simulation domain, highlighting regions of higher and lower prediction accuracy.

The objective for NOMTO was to recover the following two coupled equations from the simulation data:

$$\frac{\partial u}{\partial t} = -u \frac{\partial u}{\partial x} - v \frac{\partial u}{\partial y} + \nu \frac{\partial^2 u}{\partial x^2} + \nu \frac{\partial^2 u}{\partial y^2}, \quad (2)$$

$$\frac{\partial v}{\partial t} = -u \frac{\partial v}{\partial x} - v \frac{\partial v}{\partial y} + \nu \frac{\partial^2 v}{\partial x^2} + \nu \frac{\partial^2 v}{\partial y^2}, \quad (3)$$

where the kinematic viscosity $\nu = 2$.

To achieve this, we numerically calculated the time derivatives of the velocity components u and v , denoted as $\frac{\partial u}{\partial t}$ and $\frac{\partial v}{\partial t}$, which served as reference values for NOMTO. The inputs to NOMTO consisted of two three-dimensional arrays containing the values of u and v at the simulation grid points. The simulation grid mirrored that of the heat equation experiment, resulting in u and v arrays with shapes $(50, 50, 50)$, where the first two dimensions correspond to the spatial coordinates x and y , and the third dimension corresponds to the time coordinate t .

We evaluated two different variants of NOMTO using the same pre-trained FNO and CNO surrogates that employed in the heat equation rediscovery. In this experiment, NOMTO was configured with two symbolic layers. The library of operations for each symbolic layer included $\{id, id, \times, \times, \frac{\partial}{\partial x}, \frac{\partial}{\partial y}\}$. To accelerate the optimization process, the multiplication operations in the library were replaced with their exact counterparts, specifically PyTorch multiplications. To identify the governing equations, we utilized an optimization procedure that incorporates $\ell_{1/2}$ penalties and periodic pruning, as detailed in Section 4.3. This approach ensures that the resulting expressions remain sparse and interpretable while effectively capturing the underlying dynamics of Burgers' equations.

The resulting equations reconstructed by NOMTO-FNO are presented below:

$$\frac{\partial u}{\partial t} = -0.9u \frac{\partial u}{\partial x} - 0.9v \frac{\partial u}{\partial y} + 2.0 \frac{\partial^2 u}{\partial x^2} + 2.0 \frac{\partial^2 u}{\partial y^2}, \quad (4)$$

$$\frac{\partial v}{\partial t} = -0.93u \frac{\partial v}{\partial x} - 0.84v \frac{\partial v}{\partial y} + 2.2 \frac{\partial^2 v}{\partial x^2} + 2.1 \frac{\partial^2 v}{\partial y^2}. \quad (5)$$

NOMTO-FNO successfully identified the diffusion terms in both equations, with coefficients closely matching the original Burgers’ equation to within the first decimal place. However, the coefficients of the convective terms were slightly less precise.

In contrast, NOMTO-CNO was not able to determine the coefficients accurately. The resulting expressions did not accurately capture the diffusion and convective terms:

$$\frac{\partial u}{\partial t} = 0.5u^2 \frac{\partial u}{\partial x} + 0.1u \frac{\partial u}{\partial x} - 0.6v \frac{\partial u}{\partial y} - 6.0 \left(\frac{\partial u}{\partial x} \right)^2 + 20 \frac{\partial u}{\partial x} + 1.0 \frac{\partial^2 u}{\partial y^2}, \quad (6)$$

$$\frac{\partial v}{\partial t} = 0.7u^2 \frac{\partial v}{\partial x} - 0.5v \frac{\partial v}{\partial y} + 20 \frac{\partial v}{\partial x} + 0.9 \frac{\partial^2 v}{\partial y^2}. \quad (7)$$

The error distribution of the discovered equations is further detailed in Appendix D. Discrepancies in determining the equation coefficients may arise from several factors, including the choice of optimization strategy, use of a coarser grid compared to the simulated one, and approximation errors introduced by the neural operators within the NOMTO algorithm.

3 Discussion

This work introduces NOMTO, a novel non-linear symbolic regression algorithm that leverages neural operators to extract symbolic models from data. By incorporating sophisticated operations into its solution search space, NOMTO significantly expands the applicability of traditional symbolic regression methods. We demonstrated the algorithm’s ability to identify expressions containing derivative operations and its utility as a model discovery tool for systems governed by non-linear partial differential equations. The capability to perform immediate inference and back-propagate through differential operators enables NOMTO to efficiently explore the solution space, more efficiently compared to previous evolutionary symbolic regression approaches.

NOMTO performs well on standard symbolic benchmark expressions, and effectively handles cases involving singularities, such as division operations and the Gamma function. Although NOMTO encounters challenges in determining precise coefficients in these cases due to data clipping procedures, it successfully identifies the general structure of the expressions. This ability underscores NOMTO’s potential to handle complex operations, thereby extending the boundaries non-linear symbolic regression methods. Furthermore, NOMTO’s capacity to automatically discover non-linear models involving derivatives and special functions represents a significant advancement in symbolic regression. This is particularly evident in its application to discovering partial differential equations, as demonstrated by our experiments with the two-dimensional heat and Burgers’ equations.

However, NOMAD exhibits limitations when dealing with expressions that have low magnitudes within the search domain. This challenge can potentially be mitigated by developing more accurate neural operator surrogates that better approximate library operations across a wider range of input function magnitudes. This would directly translate to more precise resulting symbolic expressions. Furthermore, exploring more efficient sparsity-enforcing techniques and optimization strategies could further refine the algorithm’s effectiveness.

In summary, NOMTO presents a promising framework for symbolic regression and model discovery by combining the robustness and interpretability of symbolic models with generalization capabilities of neural operators. Its ability to generalize across a diverse array of functions and non-linear operators facilitates breakthroughs in fields such as fluid dynamics, materials science, biological systems modeling, and climate science. Researchers in these areas can leverage NOMTO to develop various closure models and uncover underlying governing equations from experimental or simulation data, accelerating the development of interpretable models and enhancing our understanding of complex systems.

4 Methodology

In this chapter, we first introduce the concept of the expression tree and the library of operations in Section 4.1. Next, we describe the training procedure for the neural operator blocks in Section 4.2. Subsequently, we provide a detailed overview of the overall architecture of NOMTO, including the neural operator blocks, in Section 4.3. Finally, the optimization setup and expression extraction process are discussed in Section 4.4.

4.1 Expression Tree and Library

One effective method for representing a symbolic expression is through an expression tree, a graph where each node represents an operation, variable, or constant. Before addressing the symbolic regression problem, it is essential to select a comprehensive set of symbolic operations that will constitute the expression tree. This

collection is referred to as the library, and it must include sufficient operations to adequately represent the target symbolic expression. Our approach employs a composite architecture built from different blocks, where each block corresponds to one of the library operations within the expression tree. The library includes unary operations, which require a single input argument, such as $\{id, const, \exp(\cdot), \sqrt{\cdot}, \cdot^2, \ln \cdot, \sin(\cdot), \cos(\cdot), \frac{d}{dt}\}$ and binary operations, which require two input arguments, like $\{\times, \div\}$. Where id stands for identity operation, and $const$ is an operation that always returns 1. Summation and subtraction operations are handled during the weighted sum passing between the nodes. For our initial experiment, designed to compare NOMTO with EQL and KAN on a set of common benchmark expressions, the unary operations include: $\{id, const, (\cdot)^2, \sin, \cos, \ln, \sqrt{\cdot}\}$. The binary operations selected are $\{\times, \div\}$. In subsequent experiments, the library is defined within the corresponding results subsections. Instead of directly using these exact operations, we prepare surrogate neural operator-based models for each operation in the library. These blocks are composed of neural operators, which are pre-trained to approximate the predefined library operations. The complete architecture of the proposed NOMTO approach forms a computational graph composed of multiple layers of nodes. Each node within a layer is fully connected to every node in the preceding layer, while nodes within the same layer remain unconnected. The depth of the computational graph is determined either by the number of layers or by the longest path from the output node to any input node.

4.2 Neural Operators as Surrogate Library Operations

Neural operators are a class of algorithms specifically designed to approximate nonlinear operators. Unlike traditional neural networks, which learn mappings between finite-dimensional input and output vectors, neural operators are developed to learn mappings between infinite-dimensional functional spaces [28, 29]. This capability enables them to approximate non-linear operators and compute their numerical derivatives – tasks that were previously unachievable with point-wise symbolic regression methods. Additionally, neural operators can construct differentiable surrogate models for functions with singularities by learning manually redefined versions of these functions. In this work, we utilize Fourier Neural Operators (FNOs) [25] and Convolutional Neural Operators (CNO) [23] to approximate symbolic operations. FNOs accurately capture clipped discontinuities (jumps) in discretized output functions. FNOs achieve this by learning mappings in the Fourier domain, making them particularly effective for such tasks. However, CNO have been previously shown to outperform FNO on a set of PDE benchmarks [23], making it more suitable for smoother approximations. We refer to different NOMTO variants as NOMTO-CNO and NOMTO-FNO depending on the underlying type of neural operators.

Neural operators, by design, process functions as inputs and produce functions as outputs, enabling the expansion of expression search space beyond algebraic operations. In practice, both input and output functions are discretized. We synthesize input functions for training as mixtures of random Gaussian components, with the number of components uniformly sampled from the interval [10, 50]. These input functions are discretized over 100 equidistant points in the interval $[-10, 10]$. The corresponding output functions are computed on the same discretization grid using the exact mathematical operations from the library, as illustrated in Figure 3.

To further refine the target function values, we apply the hyperbolic tangent (\tanh) function to the output function values. The choice of \tanh as the projection space is motivated by its ability to effectively handle both low- and high-magnitude values, improving the neural operator’s approximation capabilities. Unary library operations require a single input argument, so their corresponding neural operator surrogates process one discretized input function. In contrast, binary operations take two discretized inputs functions as separate input channels. Each neural operator surrogate model is trained on a dataset of 10^5 samples, ensuring a robust approximation of the respective operation.

Certain functions in the library, such as Γ and div , can produce outputs with extremely large magnitudes. To mitigate this, we project the output functions into the \tanh space. To prevent gradient explosion during the training of neural operators and subsequently during the training of the full algorithm (described in details below), we clip both the output values and the neural operator predictions to the range $[-\tanh(1000), \tanh(1000)]$.

Another implementation challenge arises from library functions like $\sqrt{\cdot}$ and $\ln \cdot$, which have undefined regions within their discretization domains. However, it is important to note that this limitation does not impact the method’s applicability to real-world data, as experimental measurements are generally well-defined across the domain of interest. The undefined regions of these functions pose challenges only during the optimization process when searching for a symbolic expression. To address this, we manually redefine the values of such library operations to ensure they are well-defined across the entire support. These redefined versions are detailed in Equation 8. The neural operators are subsequently trained to predict these redefined functions, enabling robust and consistent performance regardless of the input domain.

$$\sqrt{x} = \begin{cases} 0, & \text{if } x \leq 0, \\ \sqrt{x}, & \text{if } x > 0, \end{cases} \quad \ln x = \begin{cases} \ln |x|, & \text{if } x \neq 0, \\ -\infty, & \text{if } x = 0. \end{cases} \quad (8)$$

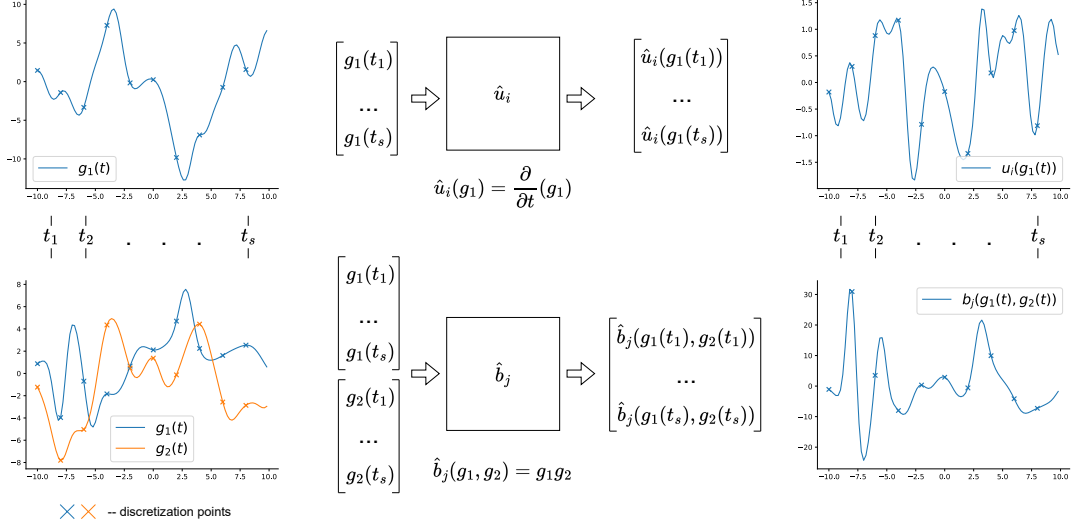


Figure 3: Construction of the Neural Operator Block.

4.3 Composing NOMTO Computational Graph

To integrate the pre-trained neural operator surrogates within the proposed framework, we construct neural operator blocks. Each neural operator block comprises either an FNO or a CNO model corresponding to a specific library function, a cropping layer, and an inverse projector denoted as \tanh^{-1} . The cropping layer ensures that predictions generated by the neural operator models remain within the range $[-\tanh(1000), \tanh(1000)]$. This constraint prevents extreme values that could destabilize the training process. Following the cropping layer, the inverse projector maps these constrained predictions back to the original functional space, maintaining the consistent and coherent function representations across different neural operator blocks. Once constructed, these neural operator blocks are integrated into the complete NOMTO architecture. Importantly, the configuration of each neural operator block remains fixed during the symbolic expression search process.

Specifically, neural operator blocks, corresponding to unary operations have one connecting edge per node in the previous layer, while nodes for binary operations have two connecting edges per node in the previous layer. In the case of binary operations, each edge represents a connection to one of the binary operation's inputs, as illustrated in Figure 1 (Step 2). The computational graph maintains a directed structure, with nodes in the last layer connected to a single output node that represents the value of the resulting symbolic expression.

Each edge in the NOMTO computational graph indicates a connection between two operations. To represent the operations' coefficients, we assign a weight $w_{ij}^{(l)}$ to the edge, connecting i -th node of layer $l-1$ to the j -th node of layer l if $j \in 1, 2, \dots, m$, and to the node $j + \lfloor (j-m)/2 \rfloor$ of layer l if $j \in m+1, m+2, \dots, m+2n$, as depicted in Figure 1. Here, m is the number of unary operations, and n is the number of binary operations in the library. The weights $w_{ij}^{(l)}$ are initialized with values drawn from a normal distribution $\mathcal{N}(0, 0.1)$ for all experiments.

4.4 Optimization and Expression Extraction

As a result, the output node of NOMTO represents the value of an expression \hat{f} , that is described by the preceding computational graph. The ground truth values of symbolic expression and the values of the output node are used to construct a loss function, defined as the ℓ_1 -norm of the prediction error $\|f - \hat{f}\|_1$. The weights on the edges of the graph are trained using the RMSProp algorithm [30]. To enforce sparsity in the model, we apply a modified $\ell_{1/2}$ -norm penalty on the network weights as an additional regularization term to the primary loss function. The modified $\ell_{1/2}$ -norm is defined as:

$$\ell_{1/2}^*(w) = \begin{cases} |w|^{1/2}, & \text{for } |w| \geq a \\ \left(-\frac{w^4}{8a^3} + \frac{3w^2}{4a} + \frac{3a}{8}\right), & \text{for } |w| < a, \end{cases} \quad (9)$$

where a is set to 0.01. Thus the total loss function becomes:

$$\mathcal{L} = \|f - \hat{f}\|_1 + \lambda \|\mathbf{w}\|_{1/2}, \quad (10)$$

where \mathbf{w} represents the set of all NOMTO's weights. In scenarios where the number of edges is relatively high, we employ periodic pruning of the weights to accelerate convergence and eliminate insignificant terms. This

approach not only promotes sparsity but also enhances the efficiency and clarity of the generated symbolic expressions. Pruning is performed on 10 % of the weights with the lowest change in their energy E during the preceding 50 epochs. The energy $E_{ij} \Big|_k$ of a weight $w_{ij}^{(l)}$ at epoch k is calculated as:

$$E_{ij} \Big|_k = w_{ij}^{(l)} \cdot \frac{\partial \mathcal{L}}{\partial w_{ij}^{(l)}} \Big|_k. \quad (11)$$

Pruning starts after 100 epochs and is conducted every 50 epochs until the number of non-zero weights reaches a predefined minimal level. The minimal number of non-zero weights is a tunable parameter that determines the desired size of the final symbolic expression.

Within the constructed computational graph, the optimized weights represent the learned symbolic expression. To extract the symbolic expression, we assign variables to each input node and sequentially apply the exact library operations, corresponding to each intermediate node. This process results in a non-linear mapping of the input variables as a combination of the library operations. It is important to note that the final expression may still contain coefficients below the 0.01 threshold, as small coefficients can accumulate through the sequential multiplication of terms. The resulting symbolic expressions are simplified using the SymPy library.

5 Data availability

The code and data required to reproduce the results will be released upon the paper’s acceptance for publication.

6 Acknowledgements

The authors gratefully acknowledge the support of the ENAC Flagship initiative at EPFL through the LASTING project and the Swiss National Science Foundation (SNSF) Grant 200021_200461.

References

- [1] Brenden K Petersen, Mikel Landajuela, T Nathan Mundhenk, Claudio P Santiago, Soo K Kim, and Joanne T Kim. Deep symbolic regression: Recovering mathematical expressions from data via risk-seeking policy gradients. *arXiv preprint arXiv:1912.04871*, 2019.
- [2] Pierre-Alexandre Kamienny, Stéphane d’Ascoli, Guillaume Lample, and François Charton. End-to-end symbolic regression with transformers. *Advances in Neural Information Processing Systems*, 35:10269–10281, 2022.
- [3] Luca Biggio, Tommaso Bendinelli, Alexander Neitz, Aurelien Lucchi, and Giambattista Parascandolo. Neural symbolic regression that scales. In *International Conference on Machine Learning*, pages 936–945. Pmlr, 2021.
- [4] Yuan Tian, Wenqi Zhou, Hao Dong, David S Kammer, and Olga Fink. Sym-q: Adaptive symbolic regression via sequential decision-making. *arXiv preprint arXiv:2402.05306*, 2024.
- [5] Martin Vastl, Jonáš Kulhánek, Jiří Kubařík, Erik Derner, and Robert Babuška. Symformer: End-to-end symbolic regression using transformer-based architecture. *IEEE Access*, 2024.
- [6] William La Cava, Bogdan Burlacu, Marco Virgolin, Michael Kommenda, Patryk Orzechowski, Fabrício Olivetti de França, Ying Jin, and Jason H Moore. Contemporary symbolic regression methods and their relative performance. *Advances in neural information processing systems*, 2021(DB1):1, 2021.
- [7] Zihan Yu, Jingtao Ding, and Yong Li. Symbolic regression via mdlformer-guided search: from minimizing prediction error to minimizing description length. *arXiv preprint arXiv:2411.03753*, 2024.
- [8] John R Koza. Genetic programming as a means for programming computers by natural selection. *Statistics and computing*, 4:87–112, 1994.
- [9] Konstantin T Matchev, Katia Matcheva, and Alexander Roman. Analytical modeling of exoplanet transit spectroscopy with dimensional analysis and symbolic regression. *The Astrophysical Journal*, 930(1):33, 2022.
- [10] Matteo Manzi and Massimiliano Vasile. Orbital anomaly reconstruction using deep symbolic regression. In *71st International Astronautical Congress*, 2020.

- [11] Baicheng Weng, Zhilong Song, Rilong Zhu, Qingyu Yan, Qingde Sun, Corey G Grice, Yanfa Yan, and Wan-Jian Yin. Simple descriptor derived from symbolic regression accelerating the discovery of new perovskite catalysts. *Nature communications*, 11(1):3513, 2020.
- [12] Mu He and Lei Zhang. Machine learning and symbolic regression investigation on stability of mxene materials. *Computational Materials Science*, 196:110578, 2021.
- [13] Ahmed M Alaa, Deepti Gurdasani, Adrian L Harris, Jem Rashbass, and Mihaela van der Schaar. Machine learning to guide the use of adjuvant therapies for breast cancer. *Nature Machine Intelligence*, 3(8):716–726, 2021.
- [14] Md Asaf-uddowla Golap, SM Taslim Uddin Raju, Md Rezwanul Haque, and MMA Hashem. Hemoglobin and glucose level estimation from ppg characteristics features of fingertip video using mggp-based model. *Biomedical Signal Processing and Control*, 67:102478, 2021.
- [15] Dimitrios Angelis, Filippos Sofos, and Theodoros E Karakasidis. Artificial intelligence in physical sciences: Symbolic regression trends and perspectives. *Archives of Computational Methods in Engineering*, 30(6):3845–3865, 2023.
- [16] Steven L Brunton, Joshua L Proctor, and J Nathan Kutz. Discovering governing equations from data by sparse identification of nonlinear dynamical systems. *Proceedings of the national academy of sciences*, 113(15):3932–3937, 2016.
- [17] Joshua S North, Christopher K Winkle, and Erin M Schliep. A review of data-driven discovery for dynamic systems. *International Statistical Review*, 91(3):464–492, 2023.
- [18] Subham Sahoo, Christoph Lampert, and Georg Martius. Learning equations for extrapolation and control. In *International Conference on Machine Learning*, pages 4442–4450. Pmlr, 2018.
- [19] Ziming Liu, Yixuan Wang, Sachin Vaidya, Fabian Ruehle, James Halverson, Marin Soljačić, Thomas Y Hou, and Max Tegmark. Kan: Kolmogorov-arnold networks. *arXiv preprint arXiv:2404.19756*, 2024.
- [20] Kunpeng Xu, Lifei Chen, and Shengrui Wang. Kolmogorov-arnold networks for time series: Bridging predictive power and interpretability. *arXiv preprint arXiv:2406.02496*, 2024.
- [21] Benjamin C Koenig, Suyong Kim, and Sili Deng. Kan-odes: Kolmogorov–arnold network ordinary differential equations for learning dynamical systems and hidden physics. *Computer Methods in Applied Mechanics and Engineering*, 432:117397, 2024.
- [22] Lu Lu, Pengzhan Jin, Guofei Pang, Zhongqiang Zhang, and George Em Karniadakis. Learning nonlinear operators via deepnet based on the universal approximation theorem of operators. *Nature machine intelligence*, 3(3):218–229, 2021.
- [23] Bogdan Raonic, Roberto Molinaro, Tim De Ryck, Tobias Rohner, Francesca Bartolucci, Rima Alaifari, Siddhartha Mishra, and Emmanuel de Bézenac. Convolutional neural operators for robust and accurate learning of pdes. *Advances in Neural Information Processing Systems*, 36, 2024.
- [24] Qianying Cao, Somdatta Goswami, and George Em Karniadakis. Laplace neural operator for solving differential equations. *Nature Machine Intelligence*, 6(6):631–640, 2024.
- [25] Zongyi Li, Nikola Kovachki, Kamyar Azizzadenesheli, Burigede Liu, Kaushik Bhattacharya, Andrew Stuart, and Anima Anandkumar. Fourier neural operator for parametric partial differential equations. *arXiv preprint arXiv:2010.08895*, 2020.
- [26] Nguyen Quang Uy, Nguyen Xuan Hoai, Michael O’Neill, Robert I McKay, and Edgar Galván-López. Semantically-based crossover in genetic programming: application to real-valued symbolic regression. *Genetic Programming and Evolvable Machines*, 12:91–119, 2011.
- [27] Maarten Keijzer. Improving symbolic regression with interval arithmetic and linear scaling. In *European Conference on Genetic Programming*, pages 70–82. Springer, 2003.
- [28] Nikola Kovachki, Zongyi Li, Burigede Liu, Kamyar Azizzadenesheli, Kaushik Bhattacharya, Andrew Stuart, and Anima Anandkumar. Neural operator: Learning maps between function spaces with applications to pdes. *Journal of Machine Learning Research*, 24(89):1–97, 2023.
- [29] Emanuele Zappala, Antonio Henrique de Oliveira Fonseca, Josue Ortega Caro, Andrew Henry Moberly, Michael James Higley, Jessica Cardin, and David van Dijk. Learning integral operators via neural integral equations. *Nature Machine Intelligence*, 6(9):1046–1062, 2024.

- [30] Geoffrey Hinton, Nitsh Srivastava, and Kevin Swersky. Neural networks for machine learning. *Coursera, video lectures*, 264(1):2146–2153, 2012.

A Predicted symbolic expressions

Table 4: Symbolic expressions recovered by Kolmogorov-Arnold Network.

Benchmark	Predicted expression
Nguyen-1	$7.30x - 0.34 \cos 0.21x - 7.29 + 0.29$
Nguyen-2	$1.08x^4 + 1.14x^3 + 0.45x^2 + 0.08x - 0.24$
Nguyen-5	$-0.16 \sin 0.60x + 8.61 - 0.19 \cos 0.62x - 2.38 - 0.96$
Nguyen-6	$0.57 \cos 0.32x - 2.66 + 0.01 \cos 0.39x - 8.81 + 0.50$
Nguyen-7	$0.84x + 0.28$
Nguyen-8	$0.86 - \frac{0.08}{(0.002x+1)^2}$
Keijzer-5	$0.56x - 0.02y - 0.13z - 1.77 \sin 0.58y + 7.81 + 7.58 \sin 0.58y - 1.6 + 0.4$
Keijzer-14	$0.55x + 0.46y - 0.18z - 4.09$

Table 5: Symbolic expressions recovered by Equation Learner.

Benchmark	Expression predicted by EQL
Nguyen-1	$9.6 \cdot (0.4x + 0.3) (0.2x^2 + 0.2) - 0.7$
Nguyen-2	$-15.5 \cdot (0.2x^2 + 0.2) (-0.3x^2 - 0.3 \sin(0.3x) + 0.2) + 0.6$
Nguyen-5	$-0.2 \sin(0.9 \sin(0.7x) + 5.7 \sin(1.5x) - 1.5) - 0.9$
Nguyen-6	$0.8 \sin(1.0x) + 0.3 \sin(0.4x + 1.4 \sin(1.0x) - 2.0 \sin(1.7x) - 9.7) + 0.5 \sin(0.5x + 1.0 \sin(1.0x) - 3.5 \sin(1.7x) - 2.9)$
Nguyen-7	$1.5x$
Nguyen-8	$0.5x + 0.2 \sin(0.6x) + 0.3$
Keijzer-5	$-$
Keijzer-14	$0.2 \sin(0.8y + 3.8 \sin(0.3x + 0.7y + 1.4z) - 7.8) + 0.7 \sin(-0.6x + 0.4y + 0.7 \sin(1.1x) + 1.6) + 1.0$

B Heat equation simulation

To generate the data for the PDE rediscovery experiment, a numerical simulation of the two-dimensional heat equation was performed. The heat equation describes the diffusion of heat in a given domain over time and is represented as:

$$\frac{\partial u}{\partial t} = \alpha \left(\frac{\partial^2 u}{\partial x^2} + \frac{\partial^2 u}{\partial y^2} \right),$$

where α is the thermal diffusivity, $u = u(x, y, t)$ is the temperature distribution as a function of spatial coordinates x and y and time t .

To numerically solve this equation, we employ the finite difference method, which approximates the derivatives in space and time using discrete values on the grid. The simulation was conducted over a two-dimensional rectangular domain of size $L_x \times L_y$ discretized into a uniform grid of $N_x \times N_y$ points, with Δx and Δy representing the grid spacing in the x - and y -directions, respectively. We have set $L_x = L_y = 20$, $N_x = N_y = 50$ and $\Delta x = \Delta y \approx 0.4081$.

The time variable was discretized using a time step $\Delta t = 0.001$ for a total simulation time $T = 5$. At each time step n , the temperature at a grid point (i, j) was updated using the following explicit finite difference scheme:

$$u_{i,j}^{n+1} = u_{i,j}^n + \alpha \Delta t \left(\frac{u_{i+1,j}^n - 2u_{i,j}^n + u_{i-1,j}^n}{\Delta x^2} + \frac{u_{i,j+1}^n - 2u_{i,j}^n + u_{i,j-1}^n}{\Delta y^2} \right)$$

The initial temperature distribution, $u(x, y, 0)$, was initialized as a mixture of 100 Gaussians with covariances uniformly sampled from the $[5, 10]$ interval. We further apply Neumann boundary conditions on the edges of the simulation domain.

The temperature field is saved with 0.1 time step during the simulation. The resulting sample of one simulation is represented by a tensor of shape $(50, 50, 50)$, where the axes correspond to the x -, y - and time-axes. In total, we prepare 1,000 simulation samples with random initial conditions.

C Burgers' equation simulation

The Burgers' equations can model various physical phenomena such as turbulence and shock wave formation. The equations are given by:

$$\begin{aligned}\frac{\partial u}{\partial t} + u \frac{\partial u}{\partial x} + v \frac{\partial u}{\partial y} &= \nu \left(\frac{\partial^2 u}{\partial x^2} + \frac{\partial^2 u}{\partial y^2} \right), \\ \frac{\partial v}{\partial t} + u \frac{\partial v}{\partial x} + v \frac{\partial v}{\partial y} &= \nu \left(\frac{\partial^2 v}{\partial x^2} + \frac{\partial^2 v}{\partial y^2} \right),\end{aligned}$$

where $u = u(x, y, t)$ and $v = v(x, y, t)$ represent the velocity components in the x - and y -directions, respectively, ν is the kinematic viscosity, and t denotes time. In this experiment, the kinematic viscosity is set to $\nu = 2$.

To numerically solve these equations, we employed the explicit finite difference method with an upwind scheme for the convection terms to enhance numerical stability in convection-dominated flows.

The simulation was conducted over a two-dimensional rectangular domain. The domain and discretization grid are completely identical to the ones that were used for the heat equation simulation (Appendix B). The time variable was discretized using a time step $\delta t = 0.001$ to satisfy the Courant-Friderichs-Lewy (CFL) condition for numerical stability. The total simulation time was $T = 0.5$. We subsample the resulting velocity fields that correspond to each simulation step with the stride of 10, which results in $N_t = 50$ time frames.

At each time step, the velocity components at a grid point (i, j) were updated using the following explicit finite difference scheme:

$$\begin{aligned}u_{i,j}^{n+1} &= u_{i,j}^n - \Delta t \left(u_{i,j}^n \frac{u_{i,j}^n - u_{i-1,j}^n}{\Delta x} + v_{i,j}^n \frac{u_{i,j}^n - u_{i,j-1}^n}{\Delta y} \right) \\ &\quad + \nu \Delta t \left(\frac{u_{i+1,j}^n - 2u_{i,j}^n + u_{i-1,j}^n}{\Delta x^2} + \frac{u_{i,j+1}^n - 2u_{i,j}^n + u_{i,j-1}^n}{\Delta y^2} \right), \\ v_{i,j}^{n+1} &= v_{i,j}^n - \Delta t \left(u_{i,j}^n \frac{v_{i,j}^n - v_{i-1,j}^n}{\Delta x} + v_{i,j}^n \frac{v_{i,j}^n - v_{i,j-1}^n}{\Delta y} \right) \\ &\quad + \nu \Delta t \left(\frac{v_{i+1,j}^n - 2v_{i,j}^n + v_{i-1,j}^n}{\Delta x^2} + \frac{v_{i,j+1}^n - 2v_{i,j}^n + v_{i,j-1}^n}{\Delta y^2} \right).\end{aligned}$$

The initial velocity fields $u(x, y, 0)$ and $v(x, y, 0)$ were initialized as mixtures of 100 two-dimensional Gaussian functions. The Gaussians were defined with random means μ_i uniformly sampled within the domain and covariance matrices $\Sigma_i = \text{diag}(\sigma_{x,i}^2, \sigma_{y,i}^2)$ with $\sigma_{x,i}, \sigma_{y,i}$ uniformly sampled from the interval $[1, 3]$. The amplitudes of Gaussians were uniformly sampled from $[-1, 1]$. The resulting initial conditions were multiplied by 0.1 coefficient to limit the initial velocities and ensure numerical stability. Next, Neumann boundary conditions were applied on all edges of the simulation domain, ensuring zero-gradient conditions on the boundaries.

In total, we prepared 1000 simulation samples, each with random initial conditions as described above. The dataset consists of tensors representing the evolution of the velocity fields u and v over time.

D Error distribution of the rediscovered Burgers' equation

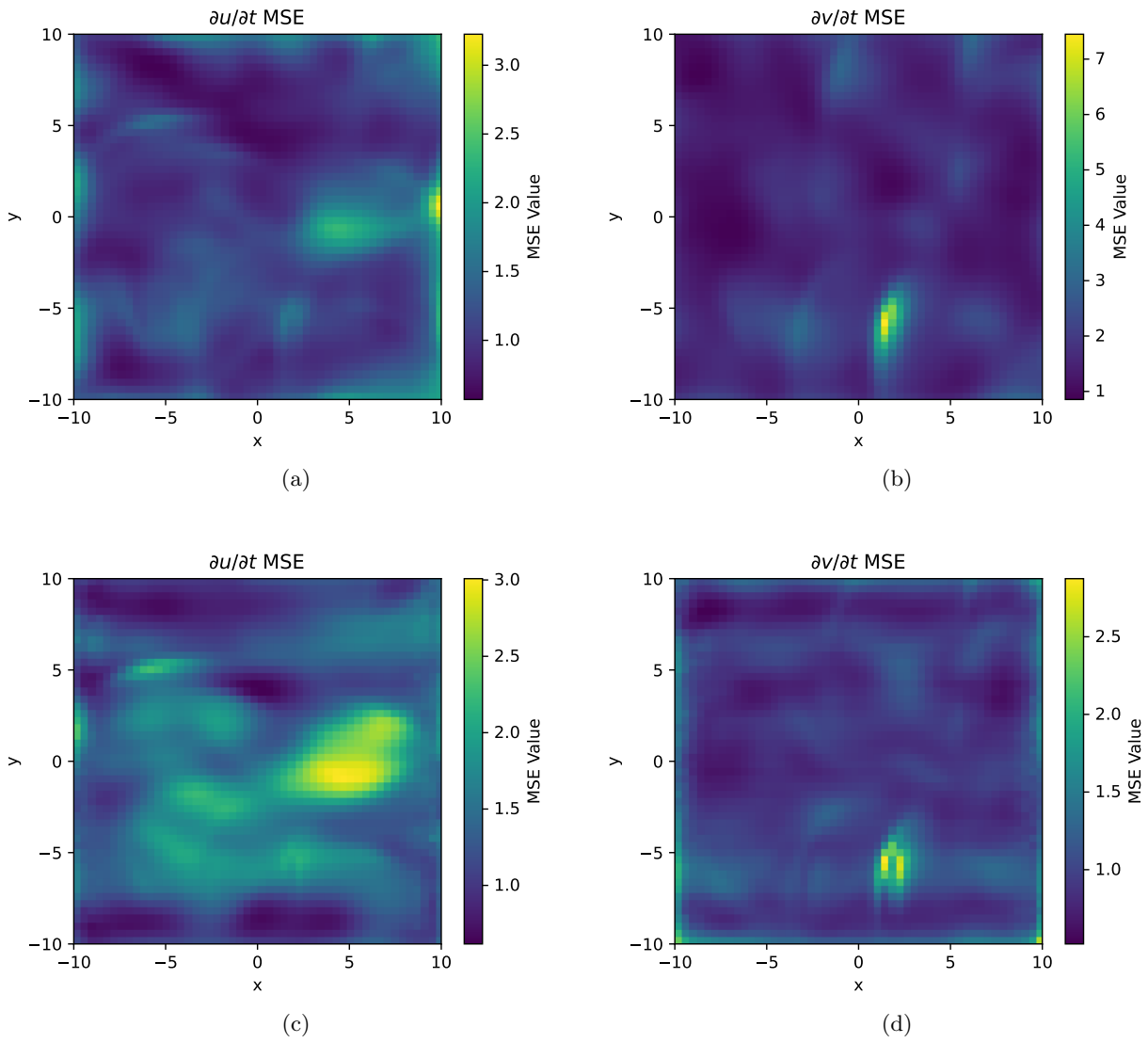


Figure 4: Prediction MSE distributions within the simulation domain: NOMTO-FNO for $\frac{\partial u}{\partial t}$ (a) and $\frac{\partial v}{\partial t}$ (b); NOMTO-CNO $\frac{\partial u}{\partial t}$ (c) and $\frac{\partial v}{\partial t}$ (d).